Isotope signature characterization of Pb and U in open air by laser-ablation mass spectrometry

Yun Shen Zhou, Yao Lu, Meng Meng Wang, Lei Liu, Xi Huang, Li Jia Jiang, Lan Jiang, Jean-François Silvain, Yong Feng Lu

ARTICLE

Isotope Signature Characterization of Pb and U in Open Air by Laser-Ablation Mass Spectrometry

Received 00th January 20xx,
Accepted 00th January 20xx

DOI: 10.1039/x0xx00000x

www.rsc.org/

Yun Shen Zhou,*[a,#] Yao Lu,[a,#] Meng Meng Wang,[a] Lei Liu,[a] Xi Huang,[a] Li Jia Jiang,[a] Lan Jiang,[b] Jean-François Silvain,[c] and Yong Feng Lu*[a]

Isotope signatures are of growing interest in recent years. In addition to the existing mass spectrometric (MS) techniques, demands on open-air and in situ analytical tools are increasing. Laser ablation is effective in atomizing and ionizing materials, and is frequently used in MS. However, light-isotope enrichment in laser-ablated plasma plumes has to be mitigated for accurate isotope analyses. In this letter, we reported an open-air laser-ablation mass spectrometric (OA-LAMS) technique to measure isotope signatures of Pb and U samples without sample pretreatments with improved accuracy in open air. The secondary cations, $PbOH^+$ and UO_2OH^+, yielded more accurate isotope signatures in regardless of environment changes. The phenomena were ascribed to the different ionization schemes, in which the primary cations came from laser ionization of the samples and the secondary cations came from chemical ionization of the ablated neutral clusters. The results demonstrated the feasibility of the OA-LAMS method in characterizing isotope signatures.

1. Introduction

Isotope signatures are of significant importance in deciphering nuclear events, tracking illicit nuclear trafficking, controlling radioactive wastes, retrieving forensic evidence, monitoring environments, dating ages, and more.[1-6] Traditionally, isotope-signature measurements were served by various mass spectrometric (MS) techniques, including isotope ratio MS (IRMS), thermal ionization MS (TIMS), secondary ion MS (SIMS), and resonance ionization MS (RIMS), which generally require sample pretreatments and controlled environmental operations.[7-21] In recent years, inductively coupled plasma mass spectrometry (ICP-MS) has been extensively investigated in isotope-signature measurements due to its relatively easy operation, high sample throughput, and simple sample preparation.[22-25] Due to the plasma instability, mass discrimination, and isobaric interferences, extra efforts, such as multicollector inductively coupled plasma mass spectrometry (MC-ICP-MS), have to be taken into consideration in obtaining accurate isotope signatures.[7, 11, 24, 26-32]

With the rapid advance of ambient ionizing techniques, such as desorption electrospray ionization and direct analysis in real time, ambient MS has received tremendous attention and experienced considerable progress in recent years.[33-35] Compared to traditional MS, ambient MS minimizes the sample pretreatments and offers unprecedented flexibility in real-time and in situ analyses.[33-35] Laser ablation has been demonstrated to be effective in atomizing and ionizing almost all materials and is, therefore, frequently used in ambient MS.[33-35] However, due to the light-isotope-enrichment effect in laser-ablated plasma plumes[36-37] and complicated matrix effects in ambient atmospheres, accurate isotope-signature analyses are extremely challenging.

In this paper, an open-air laser-ablation mass spectrometric (OA-LAMS) method was reported. Isotope signatures of Pb and U were studied in open air without sample pretreatments. The spatio-temporal evolutions of the laser-ablated plasma plumes were investigated to elucidate the ionization mechanisms underpinning the isotope-signature measurements.

2. Experimental

Samples. A commercial Pb target (99.99+%) was acquired from Kurt J. Lesker and used as received. Isotopic signatures were measured using TIMS by Geochron Laboratories (a division of Krueger Enterprises, Inc) as summarized in Table 1. Homemade U-C tablets were prepared and used. High-purity standard uranium solution (100 μg/mL in 2% HNO_3) was acquired from High-Purity Standards (a global manufacturer of NIST traceable standards for the calibration of analytical instruments) and used as received. Isotopic signatures were measured using TIMS by Geochron Laboratories as summarized in Table 1. This standard is traceable to NIST SRM 3164 and certified to ISO Guide 34 and 17025. Ultrahigh-pure graphite powder (200 mesh, 99.9999%) was acquired from Alfa Aesar and used as is. The U solution (15.0 ml) was mixed into the graphite powder (6.0 g) and milled using an agate mortar and pestle under infrared lamp irradiation. After milling, the mixture was left in a vacuum oven (80 ˚C and 5×10^{-3} torr) for 24 h to remove remaining water and HNO_3. The dehydrated powder was collected into a die set and loaded into a hydraulic press. The mixture was compressed at 5000 psi for 1 min at room temperature to form a U-C tablet with a U concentration of 250 ppm.

Table 1. Isotope signatures of the Pb and U samples measured by TIMS.

[a] *Department of Electrical and Computer Engineering, University of Nebraska-Lincoln, Lincoln, Nebraska 68588-0511, United States of America.*
[b] *Laser Micro/Nano-Fabrication Laboratory, School of Mechanical Engineering, Beijing Institute of Technology, Beijing 100081, P. R. China.*
[c] *Institut de Chimie de la Matière Condensée de Bordeaux – ICMCB-CNRS 87, Avenue du Docteur Albert Schweitzer, F-33608 Pessac Cedex, France.*
[#] The authors contributed equally to the work.
* ylu2@unl.edu and yunshen.zhou5@gmail.com
Electronic Supplementary Information (ESI) is available.

Pb Isotope Ratio*	$^{206}Pb/^{204}Pb$	21.112
	$^{207}Pb/^{204}Pb$	16.021
	$^{208}Pb/^{204}Pb$	40.480
Pb Isotope Abundance (%)*	^{204}Pb	1.272
	^{206}Pb	26.854
	^{207}Pb	20.379
	^{208}Pb	51.490
U Isotope Ratio#	$^{238}U/^{235}U$	137.548
U Isotope Abundance (%)#	^{235}U	0.722
	^{238}U	99.278

OA-LAMS system. Figure S1a shows a schematic of the OA-LAMS system that consists of three major modules: a KrF excimer laser (COMPES PRO 205 F, wavelength = 248 nm, pulse duration = 23 ns, Coherent Inc.), a time-of-flight mass spectrometer (TOF-MS, JEOL AccuTOF™, JEOL USA Inc.), and a sample stage. The excimer laser was used to atomize and ionize samples. Laser fluence was fixed at 8.75 J/cm^2, unless stated separately. The laser beam was focused at normal incidence on samples with a spot size of 0.80 × 1.60 mm^2. The AccuTOF™ MS was used as the mass analyzer. The voltages of the outer and inner orifices were fixed at 30 and 5 V, respectively. The temperature of the skimmer cone was fixed at 100 °C. The sampling distance (Figure S1b) was fixed at 2 mm, unless stated separately. The accumulation time was fixed at 1 sec for all samples. The environment relative humidity (RH) was measured by a humidity meter (00613, Acu-Rite Co Inc.) and was fixed at 40%, unless stated separately. All experiments were conducted in open air.

Imaging the laser-ablated plasma plumes. The spatio-temporal evolutions of the laser-ablated plasma plumes were recorded using an intensified charge-coupled device (ICCD) camera (ANDOR™, DH734-18U-03), which was placed perpendicular to the laser beam. Optical emission within the visible spectrum (350 – 850 nm) was recorded. A digital delay generator (Stanford Research System DG535) was used to synchronize the laser with the ICCD camera with controlled time delays. The gate width of the ICCD was fixed at 2 ns. The laser fluence was fixed at 9.02 J/cm^2. The plume images were recorded from 10 to 3700 ns immediately after the finish of the laser pulse. All experiments were conducted in open air at atmospheric pressure.

3. Results and discussion

MS measurements were conducted in open air without sample pretreatments using an OA-LAMS system (Figure S1a). To simplify the investigations and exclude unexpected interferences, a pure Pb target (99.99+%) and a home-made U-C tablet (250 ppm U in carbon) were used. In a typical OA-LAMS spectrum of the Pb target (Figure 1), Pb^+ and $PbOH^+$ of four isotopes (i.e., ^{204}Pb, ^{206}Pb, ^{207}Pb, and ^{208}Pb) are identified, in which the primary cations, Pb^+, show strong peaks at m/z of 204, 206, 207 and 208. The secondary cations, $PbOH^+$, are observed at m/z of 221, 223, 224 and 225. Due to the light-isotope-enrichment effect in the laser-ablated plasma plumes, $^{204}Pb^+$, $^{206}Pb^+$ and $^{207}Pb^+$ are obviously enriched in the OA-LAMS spectrum with significantly reduced $^{208}Pb^+$ abundance as summarized in Table 2. Surprisingly, isotope signatures in $PbOH^+$ are close to the TIMS results (Table 2). Based on the definition of IUPAC, the correction factor for mass discrimination, K, is equal to the true isotope ratio, R, divided by the observed isotope ratio.[38] The mass discrimination correction factors using Pb^+ and $PbOH^+$ were calculated respectively as listed in Table 3. As shown in Table 3, the mass discrimination correction factors were 2.315, 1.971, and 3.383 for $^{206}Pb/^{204}Pb$, $^{207}Pb/^{204}Pb$, and $^{208}Pb/^{204}Pb$ respectively calculated using Pb^+. The mass discrimination correction factors were 1.018, 0.996, and 1.036 for $^{206}Pb/^{204}Pb$, $^{207}Pb/^{204}Pb$, and $^{208}Pb/^{204}Pb$ respectively calculated using $PbOH^+$. According to the mass discrimination correction factors listed in Table 3, $PbOH^+$ delivers results much closer to the true value. Similar phenomena were observed when studying the U sample (Figure S2), in which UO_2^+ and UO_2OH^+ were observed at m/z of 267 ($^{235}UO_2^+$), 270 ($^{238}UO_2^+$), 284 ($^{235}UO_2OH^+$), and 287 ($^{238}UO_2OH^+$), respectively. The other two peaks, m/z of 286 and 288, were assigned to $^{238}UO_3^+$ and $^{238}UO_2^+H_2O$, respectively (Figure S2c). Among all observed peaks, $^{238}UO_2^+$ and $^{238}UO_2OH^+$ yielded the most and second strongest peaks, respectively. Due to its low abundance (0.722%), ^{235}U signals were barely visible in Figure S2a. Corresponding zoomed-in spectra are shown in Figures S2b and S2c, in which $^{235}UO_2^+$ and $^{235}UO_2OH^+$ were discerned at 267 and 284, respectively. Corresponding abundances of ^{235}U and ^{238}U are listed in Table 4. Similar to the results observed in Pb, the ^{235}U abundance in UO_2^+ is obviously higher than the bulky sample, but its abundance in UO_2OH^+ is very close to the bulky sample (Table 4). The relatively large measurement uncertainties (Tables 2 and 4) were ascribed to the ambient environment fluctuations. Potential influences from oxygen isotopes were not considered in this study due to the dominance of ^{16}O (abundance of 99.757%) among the natural occurring isotopes, i.e. ^{16}O, ^{17}O and ^{18}O.

In open-air laser ablation processes, ions are generated from either photoionization or chemical ionization when reacting with ambient gases. Therefore, factors that could impact either the photoionization or chemical ionization processes were investigated, including incident laser fluence, environmental relative humidity (RH), and sampling distance (as defined in Figure S1b), to study the consistency of the secondary ions, $PbOH^+$ and UO_2OH^+ in this study, in the open-air isotope-signature characterization.

Laser fluence can significantly impact the formation and propagation of laser-ablated plasma plumes and material ionization when the laser wavelength, pulse duration, and repetition rate are fixed. Figures 2a and 2b demonstrate the influence of the laser influence on Pb isotope abundances in Pb^+ and $PbOH^+$, respectively. As observed in Figures 2a and 2b, the Pb isotope abundances fluctuate up and down within the incident laser fluence range, and do not show obvious dependence on the laser fluence. In Pb^+ (Figure 2a), average abundances of ^{204}Pb, ^{206}Pb, ^{207}Pb, and ^{208}Pb were 3.12 ± 0.29, 30.21 ± 0.13, 26.37 ± 0.29, and 40.30 ± 0.41, respectively, showing obvious light-isotope enrichments. The laser-fluence inertness is also observed in $PbOH^+$ (Figure 2b). Average abundances of ^{204}Pb, ^{206}Pb, ^{207}Pb, and ^{208}Pb were 1.31 ± 0.07, 27.03 ± 0.10, 21.39 ± 0.19, and 50.27 ± 0.31, respectively, close to the TIMS results.

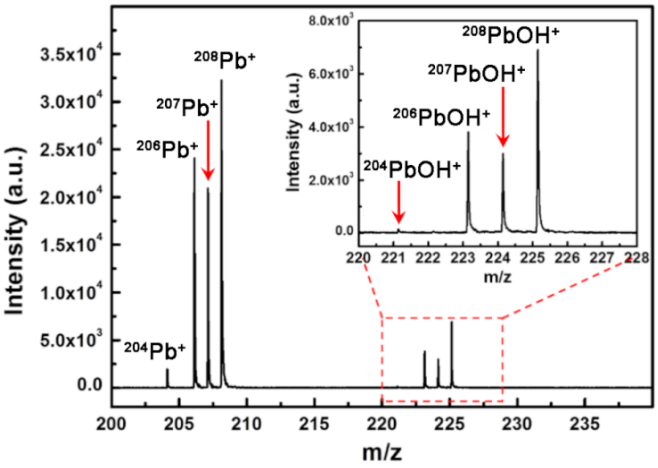

Fig. 1. A typical OA-LAMS spectrum of the Pb target at the positive ion mode showing both Pb^+ and $PbOH^+$ peaks. The inset shows a zoomed view of the $PbOH^+$ peaks.

Table 2. Pb isotope abundances obtained from TIMS, OA-LAMS-Pb^+, and OA-LAMS-$PbOH^+$, respectively.

Abundance (%)	^{204}Pb	^{206}Pb	^{207}Pb	^{208}Pb
TIMS	1.272	26.854	20.379	51.490
Pb^+	3.31 ± 0.55	30.19 ± 0.16	26.90 ± 0.28	39.60 ± 0.89
$PbOH^+$	1.30 ± 0.04	26.97 ± 0.27	20.91 ± 0.58	50.82 ± 0.57

Table 3. Correction factors for mass discrimination calculated using Pb^+ and $PbOH^+$, respectively.

	$^{206}Pb/^{204}Pb$	$^{207}Pb/^{204}Pb$	$^{208}Pb/^{204}Pb$
TIMS	21.112	16.021	40.480
Pb^+	9.121	8.127	11.964
K_{Pb^+}	2.315	1.971	3.383
$PbOH^+$	20.746	16.085	39.092
K_{PbOH^+}	1.018	0.996	1.036

As evidenced by the observation of $PbOH^+$ and UO_2OH^+, water vapor played an active role in forming the hydroxide cations. Therefore, the impacts of the environmental RHs on Pb isotopes were investigated as shown in Figure 3. The dashed lines in the figures indicate corresponding isotope abundances measured by TIMS. Similar to the results discussed above, the abundances of ^{206}Pb and ^{207}Pb were obviously increased in Pb^+, and kept almost constant in $PbOH^+$. While the abundance of ^{208}Pb was noticeably reduced in Pb^+, and kept almost constant in $PbOH^+$. In addition, the isotope abundances fluctuate within a narrow range without a consistent trend when the RH increases from 25% to 50%. Using ^{207}Pb as an example (Figure 3b), the abundance fluctuated between 26.37% and 26.66% in Pb^+, and between 21.38% and 22.06% in $PbOH^+$.

Table 4. U isotope abundances obtained from TIMS, OA-LAMS-UO_2^+, and OA-LAMS- UO_2OH^+, respectively.

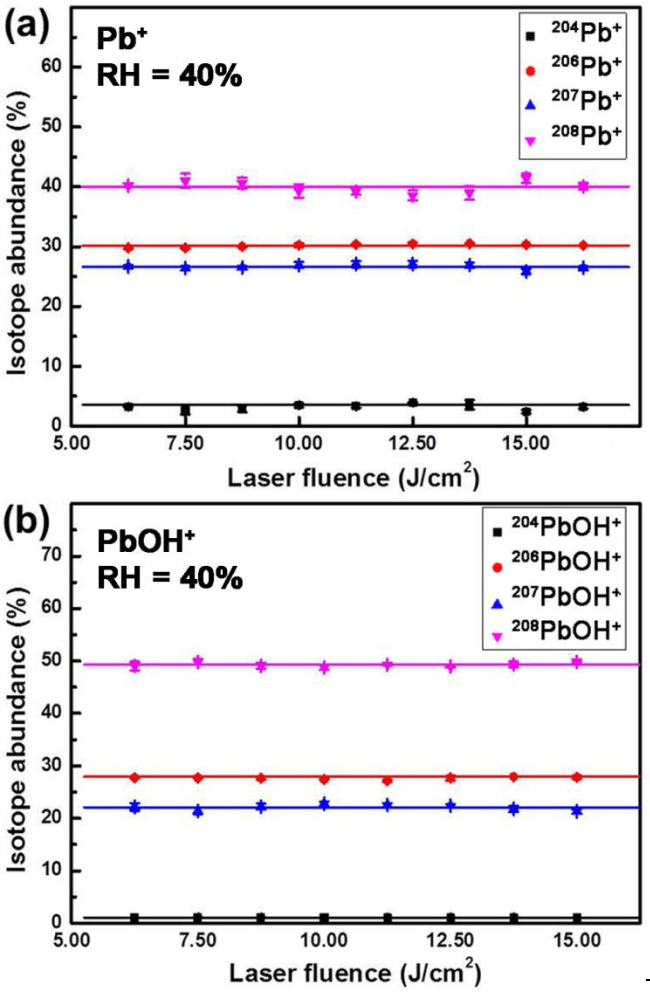

Fig. 2. Dependence of the Pb isotope abundances on the laser fluence, (a) Pb^+ and (b) $PbOH^+$.

Abundance (%)	^{235}U	^{238}U
TIMS	0.722	99.278
UO_2^+	1.70 ± 0.38	98.29 ± 0.38
UO_2OH^+	0.72 ± 0.12	99.27 ± 0.12

The third factor investigated was the sampling distance (Figure S1b), which impacted the distributions and densities of ablated species when the laser-ablated plasma plume propagated in open air. The propagation of a plasma plume is drastically different in an ambient environment than in a vacuum due to the collisions between the ablated species and ambient gases.[39-43] The mean free pathways of the ablated species in open air are much shorter (< 100 nm) than in a vacuum.[44] When colliding with ambient gas molecules, energized ions lose their charges and energy, and annihilate.[39-43] Therefore, the sampling distance is an important factor in detecting ions before they annihilate.

Figures S3a and S3b show the dependence of the Pb isotope abundances on the sampling distance retrieved from Pb^+ and $PbOH^+$, respectively. Pb^+ and $PbOH^+$ were effectively detected when the sampling distance was lower than 3.0 mm. Intensities of the Pb^+ and $PbOH^+$ peaks were significantly reduced at sampling distances above 3.0 mm and diminished above 5.0 mm. As observed in the figures, Pb

isotope abundances are insensitive to the sampling distance within the effective detection range (< 3 nm).

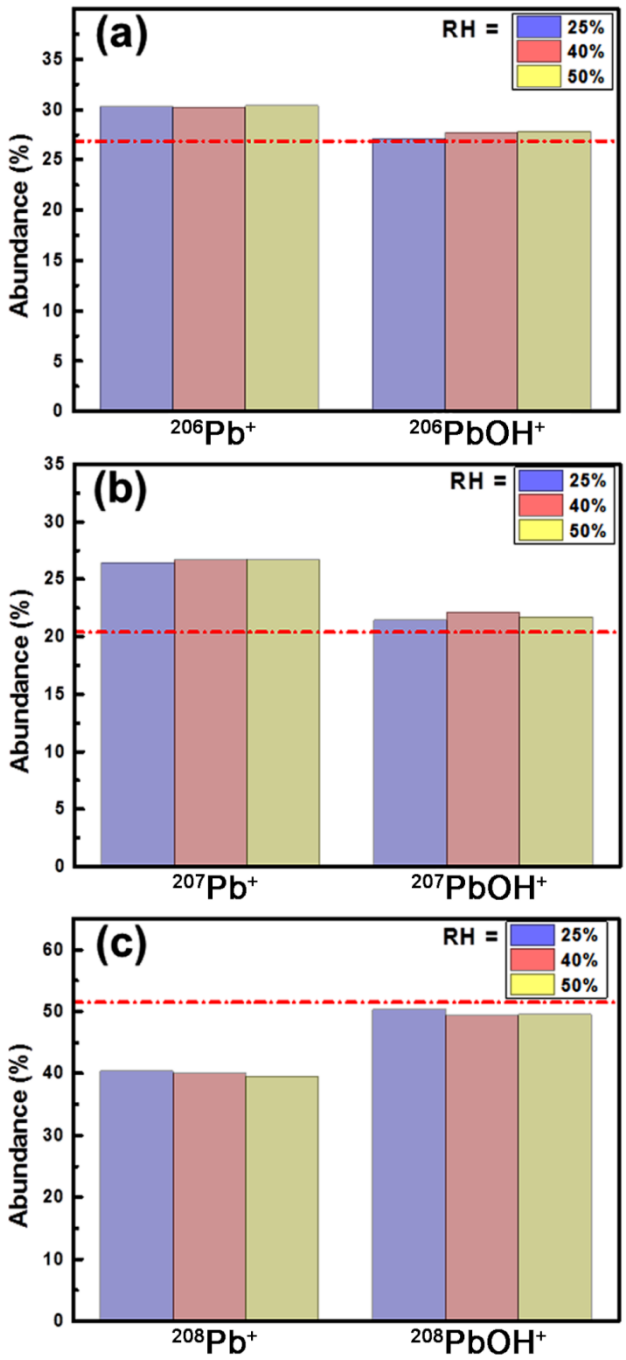

Fig. 3. Dependence of the isotope abundance on RH retrieved from Pb^+ and $PbOH^+$, (a) ^{206}Pb, (b) ^{207}Pb, and (c) ^{208}Pb.

As described above, the hydroxide cations ($PbOH^+$) delivered consistent isotope information close to the bulky sample in open air. Different from Pb^+, the isotope enrichment phenomena were minimized in $PbOH^+$. The spatio-temporal evolution of the laser-ablated Pb plasma plumes was investigated to explore the mechanisms behind the phenomena. As shown in Figure 4, hemispherical plumes were observed. The plume colors represent emission intensities that are the functions of the temperature and particle densities of the plasma plumes. A high count refers to a high temperature and particle density.[39-43]

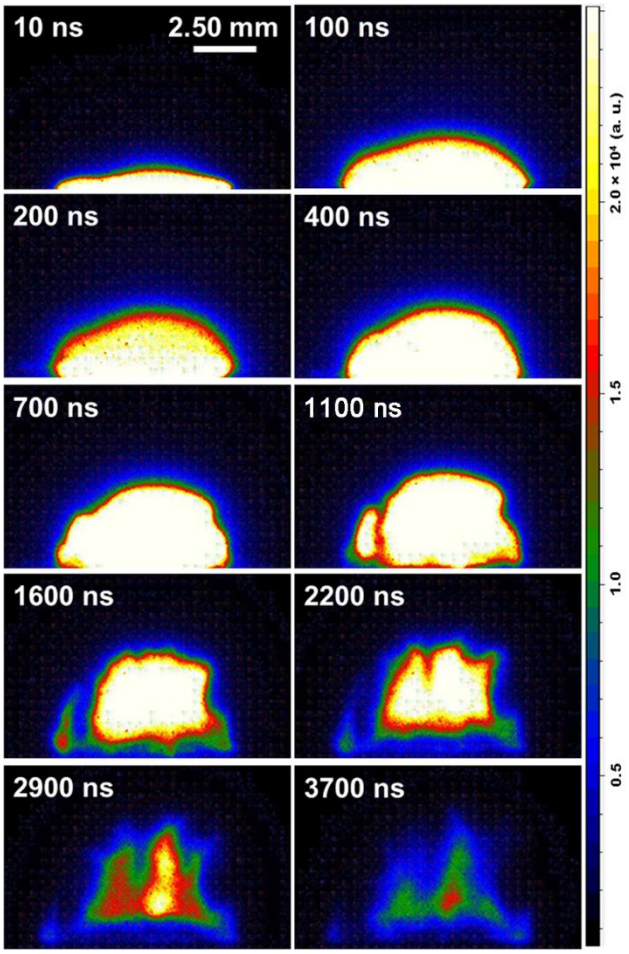

Fig. 4. Time sequence of two-dimensional ICCD images showing the spatio-temporal evolution of the laser-ablated Pb plasma plume recorded after the onset of the plasma formation. The images are normalized to the maximum peak intensity of the images for clarity.

As observed in Figure 4, the plasma plume experienced three phases sequentially: 1) plasma formation and expansion ($\leqslant$ 400 ns), 2) plasma confinement (400 – 1100 ns), and 3) plasma collapse and dissipation ($\geqslant$ 1600 ns).[39-43] In Phase 1, the plasma plume started to expand longitudinally and vertically, and reached its maximum radial size around 4.0 mm at the end of the phase. It should be pointed out that the ICCD captures emissions of the plumes. Therefore the observed boundaries are larger than the actual plasma boundaries. In Phase 2, plume confinement was observed, in which the plume reached its size and kept almost constant within the time frame. Different from laser ablation in a vacuum, ambient air exerted significant influence in the plasma plume kinetics and mitigated the energetic ions. Due to the collisional cooling and recombination processes, expansion of the plasma plume was remarkably slowed down and confined. At the same time, the confined plasma plume created a relatively enclosed environment in which the concentrations of the ablated species were kept relatively constant. In Phase 3, the plasma plume started to shrink in size and dim in color, indicating the cooling down of the plasma.

As observed in the ICCD images (Figure 4), a typical plasma plume contains two regions: plume core and plume periphery. Due to the features of a typical thermodynamic ablation process, in which the pulse duration is longer than the electron-lattice relaxation time (1 - 10 ps),[39-43] the thermal effect plays a critical role in generating the plasma. A plume core, the central part of the plasma plume, contains ions and neutral clusters resulted from laser ablation, i.e., neutral Pb clusters, Pb^+, and electrons. Due to the high temperature, pressure, and kinetic energy, chemical reactions between the ablated species and ambient gases are inevitable.[45] Therefore, a plume periphery can be treated as the interface between the ablated species and ambient air.

Since the mean free pathways of the ions were extremely short in ambient air (< 100 nm),[44] it is reasonable to suggest that the plasma plumes were the effective regions in which ions were sampled. Therefore, the effective MS sampling distance should be closely related to the plasma plume size as evidenced by the effective sampling distance (Figure S3) and the maximum plume size (Figure 4).

The different performance of Pb^+ and $PbOH^+$ was suggested to be coming from various ionization schemes. Pb^+ comes from the laser-induced photoionization of the target. Similar to the published reports,[36-37] light-isotope enrichments were observed. Due to the confinement effect in the plume expansion process, the plume core maintains a relatively enclosed environment and constant isotope signatures in Pb^+ before plasma cooling down. $PbOH^+$ comes from the chemical ionization of the neutral Pb clusters in the plume peripheries when colliding and reacting with ambient air.[45] Since the neutral Pb clusters were ablated from the bulky Pb target due to the thermal effects, they contained the same isotope signatures as the bulky target. In Chemical reactions, isotopic effects are closely related to relative masses and most pronounced when the relative mass change is greatest.[46-48] Consequently, chemical isotopic effects in heavy elements, such as Pb, are negligible, hence, were not considered. Therefore, the isotope signatures in $PbOH^+$ are very close to the bulky sample in regardless of environmental changes.

4. Conclusion

In summary, an OA-LAMS system was developed and characterized isotope signatures in open air without sample pretreatments. Different from the primary cations, Pb^+ and UO_2^+, that demonstrated obvious light-isotope enrichments, the secondary cations, $PbOH^+$ and UO_2OH^+, yielded isotope signatures close to the bulky samples in regardless of environmental changes. The consistency of the MS characterization was ascribed to the confined plasma plumes, in which the isotope signatures of the laser-ablated species were maintained before the plasma cooling down. The different performances of the primary and secondary cations were the result of the different ionization schemes. The Pb^+ and UO_2^+ were suggested to be coming from photoionization of the bulky samples, while the $PbOH^+$ and UO_2OH^+ came from the chemical ionization of the ablated neutral Pb and UO_2 clusters. The results demonstrated a potential methodology for characterizing isotope signatures in open air using the OA-LAMS method.

Acknowledgement

This work was conducted under the auspices of the Defense Threat Reduction Agency (through HDTRA1-12-1-0019 and HDTRA1-13-1-0019). The research was performed partially in the Nebraska Nanoscale Facility: National Nanotechnology Coordinated Infrastructure and the Nebraska Center for Materials and Nanoscience, which are supported by the National Science Foundation under Award ECCS: 1542182, and the Nebraska Research Initiative.

Notes and references

***** Measured ratios corrected for mass fractionation of 0.25 ± 0.02 % per atomic mass unit based on replicate analyses of NBS-981; precision of ratios is better than 0.1%.
Measured ratios corrected for mass fractionation of 0.09 % per atomic mass unit. Precision of ratios is 0.02%.

1. D. N. Correa, J. M. Santos, L. S. Eberlin, M. N. Eberlin and S. F. Teunissen, *Analytical Chemistry*, 2016, **88**, 2515-2526.
2. J. J. Bellucci, A. Simonetti, C. Wallace, E. C. Koeman and P. C. Burns, *Analytical Chemistry*, 2013, **85**, 4195-4198.
3. Z. Varga, M. Wallenius, K. Mayer, E. Keegan and S. Millett, *Analytical Chemistry*, 2009, **81**, 8327-8334.
4. E. C. Koeman, A. Simonetti and P. C. Burns, *Analytical Chemistry*, 2015, **87**, 5380-5386.
5. H. F. Cheng and Y. A. Hu, *Environmental Pollution*, 2010, **158**, 1134-1146.
6. Y. Ueno, *Geochimica Et Cosmochimica Acta*, 2010, **74**, A1062-A1062.
7. D. J. Weiss, B. Kober, A. Dalgopolova, K. Gallagher, B. Spiro, G. Le Roux, T. F. D. Mason, M. Kylander and B. J. Coles, *International Journal of Mass Spectrometry*, 2004, **232**, 205-215.
8. E. Gautier, R. Garavaglia, A. Lobo, M. Fernandez and H. Farach, *Journal of Analytical Atomic Spectrometry*, 2012, **27**, 881-883.
9. J. H. Park, K. Jeong and K. Song, *Asian Journal of Chemistry*, 2013, **25**, 7061-7063.
10. S. Richter and S. A. Goldberg, *International Journal of Mass Spectrometry*, 2003, **229**, 181-197.
11. L. V. Miller, K. M. Hambidge and P. V. Fennessey, *Journal of Micronutrient Analysis*, 1990, **8**, 179-197.
12. F. Esaka, K. Watanabe, M. Magara and S. Usuda, *Instrumentation Science & Technology*, 2004, **32**, 103-114.
13. M. Betti, *International Journal of Mass Spectrometry*, 2005, **242**, 169-182.
14. B. H. Isselhardt, M. R. Savina, A. Kucher, S. D. Gates, K. B. Knight and I. D. Hutcheon, *Journal of Radioanalytical and Nuclear Chemistry*, 2016, **307**, 2487-2494.
15. B. H. Isselhardt, M. R. Savina, K. B. Knight, M. J. Pellin, I. D. Hutcheon and S. G. Prussin, *Analytical Chemistry*, 2011, **83**, 2469-2475.
16. L. W. Green and F. C. Sopchyshyn, *International Journal of Mass Spectrometry and Ion Processes*, 1989, **89**, 81-95.
17. J. Levine, M. R. Savina, T. Stephan, N. Dauphas, A. M. Davis, K. B. Knight and M. J. Pellin, *International Journal of Mass Spectrometry*, 2009, **288**, 36-43.
18. S. L. Ziegler and B. A. Bushaw, *Analytical Chemistry*, 2008, **80**, 6029-6033.
19. H. H. Telle, A. L. Telyatnikov, E. D. Mcnaghton, R. A. Brown and A. Mccormick, *Rapid Communications in Mass Spectrometry*, 1993, **7**, 524-527.
20. I. K. Perera, *Journal of Analytical Atomic Spectrometry*, 1995, **10**, 273-280.
21. A. L. Yergey, *Journal of Nutrition*, 1996, **126**, S355-S361.

22. F. Vanhaecke, L. Moens, R. Dams, I. Papadakis and P. Taylor, *Analytical Chemistry*, 1997, **69**, 268-273.
23. J. S. Becker, *Journal of Analytical Atomic Spectrometry*, 2002, **17**, 1172-1185.
24. N. Kivel, I. Gunther-Leopold, F. Vanhaecke and D. Gunther, *Spectrochimica Acta Part B-Atomic Spectroscopy*, 2012, **76**, 126-132.
25. R. Glaus, L. Dorta, Z. G. Zhang, Q. L. Ma, H. Berke and D. Gunther, *Journal of Analytical Atomic Spectrometry*, 2013, **28**, 801-809.
26. W. M. White, F. Albarede and P. Telouk, *Chemical Geology*, 2000, **167**, 257-270.
27. T. Hirata, *Analyst*, 1996, **121**, 1407-1411.
28. R. Santamaria-Fernandez and J. C. Wolff, *Rapid Communications in Mass Spectrometry*, 2010, **24**, 1993-1999.
29. I. Segal, L. Halicz and I. T. Platzner, *International Journal of Mass Spectrometry*, 2002, **216**, 177-184.
30. I. Platzner, S. Ehrlich and L. Halicz, *Fresenius Journal of Analytical Chemistry*, 2001, **370**, 624-628.
31. M. Ohata, N. Nonose, L. Dorta and D. Gunther, *Analytical Sciences*, 2015, **31**, 1309-1315.
32. M. Guillong, P. Heimgartner, Z. Kopajtic, D. Gunther and I. Gunther-Leopold, *Journal of Analytical Atomic Spectrometry*, 2007, **22**, 399-402.
33. G. A. Harris, A. S. Galhena and F. M. Fernandez, *Analytical Chemistry*, 2011, **83**, 4508-4538.
34. M. E. Monge, G. A. Harris, P. Dwivedi and F. M. Fernandez, *Chemical Reviews*, 2013, **113**, 2269-2308.
35. Y. Lu, Y. S. Zhou, W. Qiu, X. Huang, Y. Gao, L. Liu, Y. T. Lei, T. C. Zhang, L. Jiang, J. F. Silvain and Y. F. Lu, *Journal of Analytical Atomic Spectrometry*, 2015, **30**, 1663-1667.
36. P. P. Pronko, P. A. VanRompay, Z. Zhang and J. A. Nees, *Physical Review Letters*, 1999, **83**, 2596-2599.
37. M. Joseph and P. Manoravi, *Applied Physics a-Materials Science & Processing*, 2003, **76**, 153-156.
38. T. B. Coplen, Rapid Communications in Mass Spectrometry, 2011 **25**, 2538-2560.
39. A. E. Hussein, P. K. Diwakar, S. S. Harilal and A. Hassanein, *Journal of Applied Physics*, 2013, **113**.
40. M. Thiyagarajan and J. Scharer, *Journal of Applied Physics*, 2008, **104**.
41. M. Cirisan, J. M. Jouvard, L. Lavisse, L. Hallo and R. Oltra, *Journal of Applied Physics*, 2011, **109**.
42. S. B. Wen, X. L. Mao, R. Greif and R. E. Russo, *Journal of Applied Physics*, 2007, **101**.
43. S. B. Wen, X. L. Mao, R. Greif and R. E. Russo, *Journal of Applied Physics*, 2007, **101**.
44. S. G. Jennings, *Journal of Aerosol Science*, 1988, **19**, 159-166.
45. K. Sasaki and H. Watarai, *Japanese Journal of Applied Physics Part 2-Letters & Express Letters*, 2006, **45**, L447-L449.
46. J. Bigeleisen, *Journal of the American Chemical Society*, 1996, **118**, 3676-3680.
47. F. S. Klein, *Annual Review of Physical Chemistry*, 1975, **26**, 191-210.
48. R. E. Weston, *Annual Review of Nuclear Science*, 1961, 11, 439-460.